How minute sooglossid frogs hear without a middle ear

Renaud Boistel[a,b,c,1], Thierry Aubin[a,b], Peter Cloetens[d], Françoise Peyrin[d,e], Thierry Scotti[f], Philippe Herzog[f], Justin Gerlach[g], Nicolas Pollet[h], and Jean-François Aubry[i]

[a]Centre de Neurosciences Paris-Sud (CNPS), Centre National de la Recherche Scientifique (CNRS) Unité Mixte de Recherche (UMR) 8195, Université Paris XI, 91405 Orsay, France; [b]Université Paris Sud, 91405 Orsay, France; [c]Institut International de Paléoprimatologie et de Paléontologie Humaine (IPHEP), CNRS UMR 7262, Université de Poitiers, F-86022 Poitiers, France; [d]European Synchrotron Radiation Facility, 38043 Grenoble, France; [e]Centre de Recherche en Acquisition et Traitement de l'Image pour la Santé, CNRS UMR 5515, Institut national des sciences appliquées de Lyon, 69621 Villeurbanne, France; [f]Laboratoire de Mécanique et d'Acoustique (LMA), CNRS UPR 7051, 13402 Marseille, France; [g]Nature Protection Trust of Seychelles, Victoria, Mahé, Seychelles; [h]Institute of Systems and Synthetic Biology, Genopole, CNRS, Université d'Evry Val d'Essonne, F-91058 Evry, France; and [i]Institut Langevin, CNRS UMR 7587, École supérieure de physique et de chimie industrielles de la ville de Paris ParisTech, 75005 Paris, France

Edited by David B. Wake, University of California, Berkeley, CA, and approved August 1, 2013 (received for review February 7, 2013)

Acoustic communication is widespread in animals. According to the sensory drive hypothesis [Endler JA (1993) *Philos Trans R Soc Lond B Biol Sci* 340(1292):215–225], communication signals and perceptual systems have coevolved. A clear illustration of this is the evolution of the tetrapod middle ear, adapted to life on land. Here we report the discovery of a bone conduction–mediated stimulation of the ear by wave propagation in *Sechellophryne gardineri*, one of the world's smallest terrestrial tetrapods, which lacks a middle ear yet produces acoustic signals. Based on X-ray synchrotron holotomography, we measured the biomechanical properties of the otic tissues and modeled the acoustic propagation. Our models show how bone conduction enhanced by the resonating role of the mouth allows these seemingly deaf frogs to communicate effectively without a middle ear.

earless frog | audition | extra-tympanic pathways | X-ray imaging

The middle ear evolved multiple times independently during the evolution of terrestrial life (1). Indeed, a tympanic middle ear is an adaptation to life on land (2, 3) and compensates for the mismatch in acoustic impedance between air and tissue. Without it, 99.9% of sound energy is reflected by the body wall (4, 5). *Sechellophryne gardineri* is one of the world's smallest terrestrial tetrapods (6). These sooglossid frogs have a Gondwanan origin and evolved in isolation on the Seychelles Archipelago over the last 47–65 My (7, 8). They lack a middle ear yet produce acoustic signals (9, 10). In fact, similar to many species of frogs lacking the tympanic middle ear, they are still capable of hearing in air. Nevertheless, the mechanisms for sound transfer to the inner ear are far less clear. Some extratympanic pathways (11) such as the lungs (12), the opercular system (13), and bone conduction (14) have been proposed but remain to be tested experimentally (11). X-ray synchrotron holotomography of a female *S. gardineri* reveals that the pulmonary system is poorly developed and cannot contribute significantly to a lung-based sound transmission pathway. We used finite-difference simulations to investigate possible pathways through the head itself. These simulations highlighted the role of the mouth. Finite-element simulations further showed that the oral cavity of the animals resonates at the dominant frequency of the advertisement call of the species. In addition, synchrotron holotomography performed on seven different species showed that earless frogs are specialized for sound transmission between the oral cavity and the ears in two ways: (*i*) by minimizing the tissue thickness between the mouth and the inner ear and (*ii*) by minimizing the number of layers of tissue. The combination of these extratympanic pathways allows the frog to perceive sound efficiently.

Results

Playback Experiments and Call Analysis. We recorded vocalization patterns of *S. gardineri* (Fig. 1*A*, Table S1, and Audio S1) in the field on Silhouette Island. The average call duration (note) is 185.14 ± 27.31 ms; call rate varied from one call every 3 min to one call every 30 min. Spectral analysis of the vocalization shows that the notes consist of a series of one to six harmonic frequencies, with a fundamental frequency of 1,830 Hz (number of calls, $n = 21$). The dominant frequency varies between 4,225 and 6,767 Hz, corresponding to the first and second harmonics, with an average frequency of 5,710 ± 420 Hz ($n = 52$). Peaks of higher frequency rarely exceed more than 10,105 Hz (Fig. 1*A*). Interestingly, we did not detect any frequency or amplitude modulation of the call. Each of the acoustic playback experiments with conspecific calls ($n = 15$) in the natural habitat of the frogs provoked vocalizations of several males, suggesting that these frogs are capable of hearing. Furthermore, males did not respond to nonspecific calls, suggesting good acoustic discrimination abilities.

Ear Anatomy. *S. gardineri* possesses no tympanum, middle ear cavity, or a columella as can be seen on the X-ray holotomographic images (Fig. 1). The inner ear is covered by a strongly ossified operculum (76% of the volume; Fig. 1*D*) at the large oval window (area: 0.677 mm^2; Fig. 1*E*). This ossicle connects to the ventral surface of the posterior suprascapula through the opercular muscle (Fig. 1*F*). The latter inserts on the operculum postero-dorsally on a narrow ridge with an asymmetrical cone-shaped aspect in profile (Fig. 1*D*). The inner ear is fully surrounded by the ossified otic capsule (Figs. 1 *B*, *F*, and *G* and 2 *A* and *B*), which contains six foramina including four in the medial wall (communicating with the endocranial cavity) and two on the posterior wall (Fig. 1 *C*, *E*, and *G*). Three points are notable

Significance

Gardiner's Seychelle frog, one of the smallest terrestrial tetrapods, resolves an apparent paradox as these seemingly deaf frogs communicate effectively without a middle ear. Acoustic playback experiments conducted using conspecific calls in the natural habitat of the frogs provoked vocalizations of several males, suggesting that these frogs are indeed capable of hearing. This species thus uses extra-tympanic pathways for sound propagation to the inner ear. Our models show how bone conduction is enhanced by the resonating role of the mouth and may help these frogs hear.

Author contributions: R.B., T.A., P.H., N.P., and J.-F.A. designed research; R.B., P.C., T.S., J.G., N.P., and J.-F.A. performed research; R.B., P.C., F.P., T.S., and J.-F.A. analyzed data; and R.B., T.A., P.C., F.P., T.S., P.H., J.G., N.P., and J.-F.A. wrote the paper.

The authors declare no conflict of interest.

This article is a PNAS Direct Submission.

[1]To whom correspondence should be addressed. E-mail: renaud.boistel@univ-poitiers.fr.

This article contains supporting information online at www.pnas.org/lookup/suppl/doi:10.1073/pnas.1302218110/-/DCSupplemental.

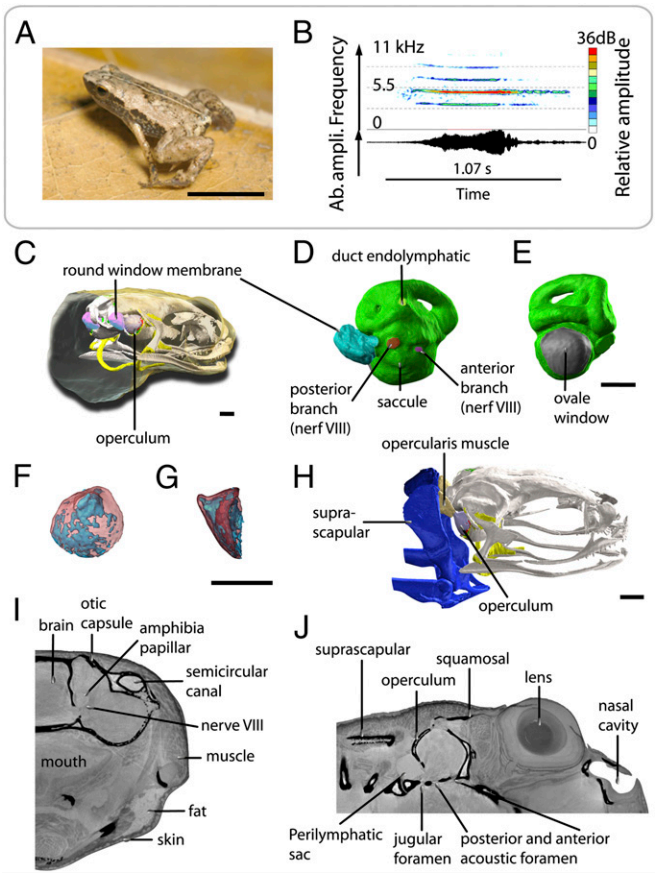

Fig. 1. Acoustic behavior and volume rendering of ear region of *S. gardineri*. (*A*) Picture of one adult male of *S. gardineri*. (*B*) Oscillogram (*Lower*) and sonogram (*Upper*) of the advertisement call. (*C*) 3D visualization of the operculum and endolymphatic sac of the oval window in the head, in 3/4 posterior view with the skin made transparent. (*D*) Median view of the inner ear (in green) with the endolymphatic sac connected to the left round window, showing the location of the posterior (red) and anterior (violet) branches of nerve VIII, the endolymphatic duct (pale green), and extracranial lymphatic sac (blue-green). (*E*) Posterior view of the left inner ear, showing the surface occupied by the oval window (in gray). (*F* and *G*) 3D visualization of the operculum in transparency (bone in red, cartilage in blue): posterior (*F*) and lateral (*G*) views. (*H*) 3D 3/4 lateral view of the opercular system with the opercular muscle shown in pink. (*I* and *J*) Sagittal and frontal sections of holotomographic images showing the foramen of the otic capsule, the innervation of the inner ear, and the organization of the tissues surrounding the ear. (Scale bar, 0.5 mm.)

regarding these foramina. First, the oval window is very large compared with that of other Anura, covering 8.5% of the surface of the inner ear. Second, the eighth cranial nerve presents a significant expansion of its posterior branch that innervates the auditory papilla. Third, an endolymphatic vessel is present as an extension of the inner ear outside the skull at the level of the oval window (Fig. 1 *A*, *C*, and *G*).

Anatomy and Morphometry. The anatomical and morphometric data extracted from holotomography reconstruction show a number of anatomical characteristics that may be involved in sound reception. Four exceptional anatomical points may have an impact on the hearing. First, the tissues surrounding the otic region have a density close to that of water (Fig. S1). There is, therefore, a high impedance gap between the air and the soft tissues. Second, the degree of mineralization of the skull (Fig. 2*A*) in this region is uniform but two to three times lower than is observed in the corresponding regions in humans and mice (15, 16). Third, the ossification is very extensive, with cartilage comprising only 18.2% of the volume (Fig. 2*B*). Fourth, the tissues separating the internal ears from the gaseous medium are extremely thin (about 40 μm), both dorsally above the semicircular canals and ventrally toward the mouth under the saccule (Fig. 2*C*). In the absence of a middle ear region, it may be possible for sound to be transmitted to the inner ear through organs such as the lungs (12). However, the 3D reconstruction of a female *S. gardineri* (Fig. 2*D*) revealed that the volume of the pulmonary system is smaller than the volume of the oral cavity (2.11 and 3.52 mm^3, respectively) and that the lung with only a single air sac is not in contact with lateral body wall, thus strongly limiting sound transmission. Consequently, the hypothesis that these frogs use a lung-based sound transmission (12) appears rather unlikely.

Bone Conduction Simulation. Using the holotomographic images of *S. gardineri*, we extracted speed and density maps of the tissues and used these as input for a finite-difference simulation of the sound propagation through the head (Fig. S2). Attenuation was measured by calculating the ratio between the pressure measured in the inner ear and the pressure outside the head. It was relatively constant as a function of frequency, with attenuation values of −27.23 dB at 5 kHz, −27.61 dB at 10 kHz, and −26.76 dB at 20 kHz (Fig. 3). The maximum pressure wave is localized in the lateral regions of the head at the level of the inner ears (Fig. 3*C* and Fig. S3). However, the presence of the mouth appears to distort the propagation of the sound wave. To compare our results with a human model, we also simulated sound propagation through a human head. Speed and density maps were extracted from a CT scan, and attenuation was calculated. CT slices were chosen dorsal to the ear canal to simulate heads without outer ears as this allowed us to evaluate the theoretical attenuation of sound by bone. The attenuation was similar in humans and frogs (−29 dB at 5 kHz) and is similar to the protection offered by a foam plug plus a small earmuff (17). The fact that the degree of attenuation in *S. gardineri* is close to that in humans indicates that size is not a major factor. Rather, impedance matching seems to be more significant, as a lower number of layers separating the inner ear from the oral cavity in earless vs. eared (Table S2) avoids corresponding impedance jumps. This impedance matching is likely to facilitate sound transmission between the oral cavity and the inner ear of earless frogs.

Modal Simulation of Oral Cavity. Transmission by bone conduction in these earless anurans is not sufficient in itself to explain their hearing capacity. Biased to their optimal operating range by noise (as in stochastic resonance) (18), the active elements in the sensory cells are able to amplify the power of the very weak vocalization signal (19). To investigate whether resonating body parts could further amplify sound, a numerical simulation of the resonating capacity of the oral and nasal cavities, as well as the open nostrils, was conducted (Fig. 3*D*). The finite-element grid of the mouth was constructed by connecting the nasal cavity to a parallelepipedic volume that permits conservation of the geometry of the nasal openings. The results are presented in Fig. 3*D* and show that only the oral cavity has the ability to resonate at 5,738 Hz, a value close to the dominant frequency present in the call of this species. In contrast, the resonating capacity of the lung is significantly higher (Fig. S4), in the ultrasound domain (58,203 Hz). Thus, for *S. gardineri*, the finite-element simulations indicate that the oral cavity, and not the lung, provides an alternative to the vocal tract as a resonator. This result is consistent with results obtained for frogs (20, 21) and other vertebrates [humans (22) and birds (23)] and confirms the hypothesis of extratympanic pathways in earless frogs (24).

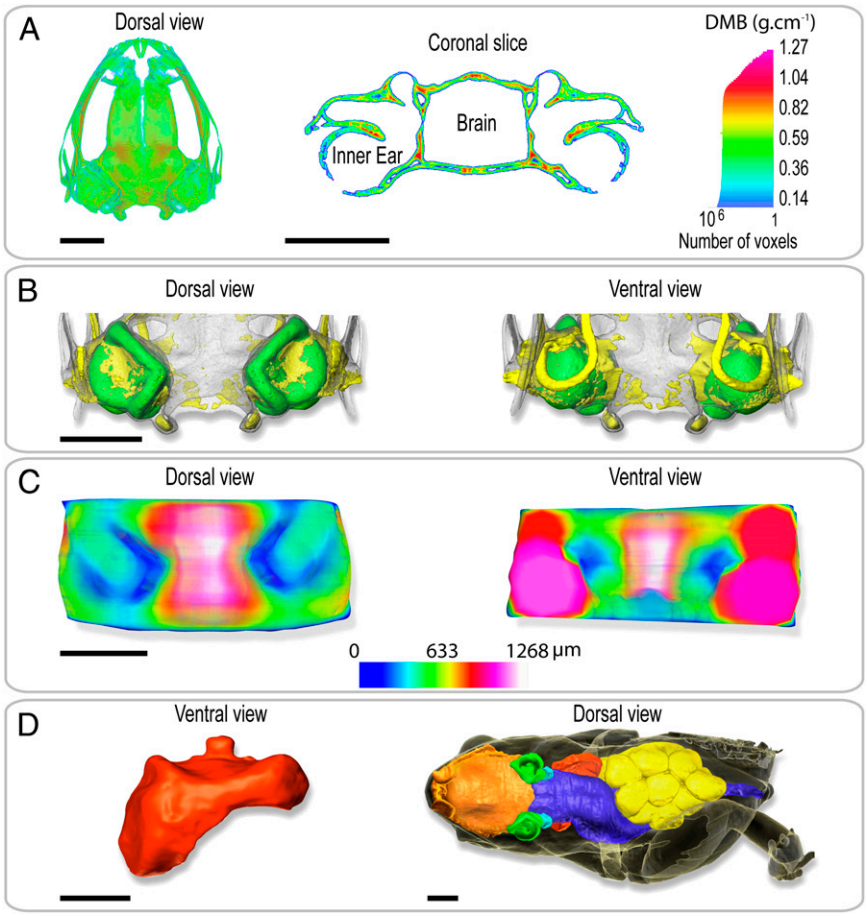

Fig. 2. Volume rendering of holotomography of the body and the tissues surrounding the ear of *S. gardineri*. (*A*) 3D map (*Left*) and virtual sagittal section (*Right*) illustrating the degree of mineralization of the skull as determined by absorption tomography. (*B*) Visualization of the degree of ossification of the otic region of the skull in dorsal (*Left*) and ventral (*Right*) views. The skull is transparent, cartilage is shown in yellow, and the inner ears in green. (*C*) 3D map of the thickness of the tissues separating the inner ears and the gaseous medium. (*Left*) Dorsal view and (*Right*) ventral view of the oral region. The thinnest parts are shown in dark blue. (*D*) 3D visualization of the pulmonary system of a gravid female (SVL = 11.65 mm). Red, pulmonary and laryngeal cavity in ventral view. To right, dorsal view of female in transparency visualizing the anatomy and the volume occupied by the nasal and oral cavities (orange), the inner ears (green), the digestive system (blue), the ovarian masses (yellow), and the pulmonary system. Note the left forelimb was removed for molecular analysis. (Scale bar, 1 mm.)

Discussion

Frogs without middle ears lack specializations to make hearing more efficient (25) and may need to compensate for the lack of the middle ear.

The ability of earless frogs to hear has been debated even though Loftus-Hills (26), Jaslow and Lombard (27), and Lindquist et al. (28) already demonstrated that some earless frogs actually have a hearing capacity comparable, in both range and sensitivity, to species with tympanic ears. To explain this observation, extratympanic pathways for sound transmission have been proposed involving the opercularis system (13), a lung-based pathway (28, 29), and a bone-based pathway (14). *S. gardineri* is an example of frog without a tympanic middle ear. It produces an advertisement call around 5,710 Hz and responds noticeably to playbacks of these calls. Our holotomography analysis shows that the opercularis system of this species is well developed, but the hearing function of this structure has still not been conclusively resolved (11, 30) and would be limited to frequencies <1 kHz (13).

The lung-based hearing hypothesis was originally proposed for eared species by Narins and coworkers (29) and later was extended to earless frogs (28). The suggestion that this system could work for earless frogs was based on data showing that the lateral body wall overlying the lung vibrates in response to airborne sounds with a frequency corresponding to the dominant frequency of the advertisement call in an earless frog (*Atelopus*) (28). A lung-based hearing system for *S. gardineri* is not supported by our holotomography and finite-element analyses. In fact, the lack of lateral body pathway and a weak development of the lung, with a volume 40% lower than that of the oral cavity, lead to resonant frequencies in the ultrasound domain, incompatible with the frequencies perceived by the species.

Bone conduction could thus constitute an alternative pathway, specifically in small animals. In the initial phase of our study, 3D finite-difference simulations were conducted to test this hypothesis. Nevertheless, in our species, bone conduction appeared to be insufficient to explain significant sound transfer to the inner ear: a drastic sound attenuation (−29 dB) was observed in our model, independent of the size and degree of mineralization of the skull. Interestingly, in the same simulations, the acoustic pressure appeared to pop up in the mouth cavity (Fig. 3*C*). Consequently, the role of the oral cavity as a resonator was investigated and shown to resonate at 5,738 Hz, a value close to the dominant frequency present in the call of this species. Thus, the oral cavity appears as the ideal frequency-tuned candidate to amplify the acoustic signal (20). Finally, the tissues separating

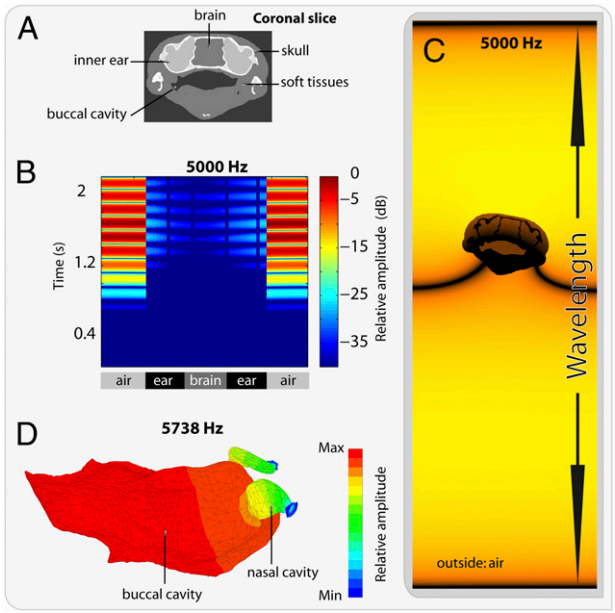

Fig. 3. Bone conduction in *S. gardineri*. (*A*) Image segmentation at the level of the inner ears used for bone conduction simulations. (*B*) Graphic representation of the acoustic pressure as a function of time (ms) along a line crossing the two inner ears; color bar shows the relative pressure amplitude in decibels. (*C*) Snapshot of the simulated field: visualization of the propagation of a pressure wave (at 5 kHz) on a coronal section of the skull. (*D*) Finite-element acoustic mode of the oral cavity and the nasal cavities with open nostrils in a 3/4 dorsal view. Color scale represents the acoustic pressure in Pascals.

the inner ear from the air cavity in the mouth are extremely thin (~80 μm) in these frogs, both dorsally above the semicircular canals and ventrally toward the mouth under the saccule (Fig. 2*C*), thus facilitating transmission from the resonator to the inner ear. This hypothesis was further investigated by measuring the distance between the mouth resonator and the inner ear for four earless frogs and three eared frogs of comparable size and for which holotomographic data were available (Table S2). Earless frogs have lower total tissue thickness between the oral cavity and the inner ear and a reduced number of interfaces, which both optimize transmission between the ear and the mouth. The role of the oral cavity as resonator, in association with bone conduction from the mouth to the inner ear is an original solution to hearing without a middle ear derived from preexisting anatomical structures and constitutes an interesting example of an exaptation (31). Aertsen and coworkers (20) and Palmer and Pinder (21), demonstrated the role of the oral cavity in rendering the coupling of eardrums asymmetric to account for the directionality of sound for hearing in frogs. We show here the enhancing role of the resonating mouth cavity in earless frogs, but the mouth could additionally play a role in detecting the directionality of sound for such earless frogs.

Our results contribute to an understanding of the evolution of the auditory system in tetrapods. It is commonly accepted that the evolution of the middle ear is associated with the transition from an aquatic to a terrestrial lifestyle. However, recent work on the earliest tetrapods has shown that these animals (32) possessed a specialized ossicle in the middle ear despite their largely aquatic lifestyle (33, 34). Furthermore, the tetrapod middle ear, with a tympanum, evolved independently at least four times in terrestrial tetrapods (35–37). We show that the presence of a middle ear is not a necessary condition for terrestrial hearing, despite being the most versatile solution for life on land (12, 24).

Methods

Study Site. Seychelles frogs were studied in the field at two locations in the Seychelles Islands: between April 9 and 29, 2002, at Jardin Marron and Anse Mondon on Silhouette Island (4°51′N; 53°3′W, 300- to 500-m elevation; 4°28′15″S, 55°13′40″E, 300-m elevation). Recording and playback experiments were undertaken during the active phonation period of males (i.e., between 6.00:00 AM and 9.30:00 PM).

Electro-Acoustic Material. Calls were recorded at 1-m distance using an omnidirectional Brüel and Kjær serial 4053 microphone mounted on a 2.5-m boom and a Sony TCD-D100 digital audio tape (DAT) recorder (sampling rate= 48 kHz, frequency response flat within the range 20–20,000 Hz). Calls were analyzed with the Syntana signal processing software (38). Frequency measurements were performed on power spectra with the following fast Fourier transform (FFT) values: Hamming window, window size = 4,096 points, filter bandwidth = 120 Hz ($T = 1/F = 8.3$ ms). Sound pressure level (SPL in dB) measurements were taken by a Bioblock Scientific Sound Level Meter type 5017 (linear frequency scale, fast setting). For playback tests, signals were played back by a Sony WM6 recorder (frequency range, 30–20,000 Hz ± 1 dB) connected to a Sony SRS-Z500 loudspeaker (frequency response, 100–16,000 Hz ± 1.5 dB).

Call Analysis. Patterns of interindividual variability of advertisement calls were assessed by analyzing 52 signals of 10 calling males. Call duration (Cd), the fundamental frequency (f0), and the dominant frequency (Df) were extracted. For each call parameter, we determined the mean, SD, minimum, and maximum.

Playback Design. Before a test, a speaker was placed at a distance of 1.5 m from the subject. To test the species-specific recognition, males were stimulated by a loudspeaker emitting two series of signals separated by a 2-min silent period. One series (the control series) consisted of conspecific calls and the other one (the experimental series) with *Eleutherodactylus martinicensis* calls. Each series consisted of 15 consecutive advertisement calls separated by artificial intercall silences (mean duration: 2.5 s). The order of presentation of both control and experimental series was randomized. In natural conditions, the response to an advertisement call was characterized by an obvious behavioral change in the male's attitude: calling in reply. On the basis of these observations, the intensity of responses of tested males to playback signals was evaluated.

Holotomography. One male and one female adult *S. gardineri*, one *Sechellophryne pipilodryas*, *Sooglossus sechellensis*, and *Sooglossus thomasseti* from Silhouette Island (Seychelles), and *Eleutherodactylus barlagnei*, *Eleutherodactylus johnstonei*, *E. martinicensis*, and *Eleutherodactylus pinchoni* from Guadeloupe Island were euthanized by an overdose of anesthetic (ketamine), fixed in 3.7% (wt/vol) formaldehyde solution, and placed in a small polypropylene tube for holotomographic imaging on return from the field. Protocols were approved by the ethics committee at the University of Paris XI. Animals were collected under collecting permits from the Seychelles Bureau of Standards and National Park of Guadeloupe. The quantitative X-ray phase contrast imaging [holotomography (39)] used the experimental station ID19 of the European Synchrotron Radiation Facility (Grenoble, France), on a long (150 m) imaging beamline with large spatial coherence of the beam. The X-ray photon energy was set to 20.5 keV with an exposure time of 0.5 s per image. Twelve hundred radiographic images with a 2,048 × 2,048 pixel resolution were acquired by a FReLoN CCD Camera (40). The effective pixel size at the converter screen position was 7.5 μm, resulting in a field of view of 15 × 15 mm^2. The data set for a single sample comprised four angular scans, recorded at different sample detector distances (40, 300, and 995 m) and chosen to avoid consistently low values of the optical transfer function for some spatial frequencies. The retrieved phase maps (Fig. S2) were used as input to a filtered backprojection tomography reconstruction algorithm yielding the distribution of the electron density and a good approximation of the mass density. Volume renderings were obtained after segmentation by using isosurface representations and volume texture renderings with Avizo from VSG.

Geometrical and Quantitative Measurements. Geometrical and quantitative measurements of the sample were performed with ImageJ. The computation of 3D direct head thickness between inner ear and air was based on the calculation of the local thickness map and was implemented using the 3D Chamfer discrete distance (16). The mean degree of mineralization of bone (DMB, g/cm^3) was derived from the distribution of the X-ray attenuation coefficient in the absorption tomography scans corresponding to the first sample detector distance. Attenuation coefficients were converted

to volumetric tissue mineralization expressed as grams per centimeter cubed of hydroxyapatite crystals, as detailed in ref. 15. Quantitative measurements on the image datasets were performed with ImageJ. 3D regions of interest are selected on the skull (angulosplenial, otic capsule, columella, squamosal, operculum, parasphenoid, and pterygoid) and soft tissues (muscles: *depressor mandibulae*, opercular, *levator mandibulae posterior longus*, and *depressor mandibulae*; cartilage: menckelien, hyale, opercular, pectoral, omosternum, *crista paraotica*, and diploe; brain; skin; and tongue).

Numerical Simulation. Simulations were performed with a finite-differences program developed at the Institut Langevin (Paris, France). It solves the 3D linear wave equation in heterogeneous and absorbing media

$$\left\{\rho_0\left(\vec{r}\right)\nabla\cdot\left[\frac{1}{\rho_0\left(\vec{r}\right)}\nabla p\left(\vec{r},t\right)\right]\right\}-\frac{1}{c_0\left(\vec{r}\right)^2}\frac{\partial^2 p\left(\vec{r},t\right)}{\partial t^2}=S_0\left(\vec{r},t\right),$$

where $c_0(\vec{r})$ is the speed of sound, and $\rho_0(\vec{r})$ is the density. Simulations were conducted for frequencies ranging from 5 to 40 kHz. The simulation grid was set to 1/10th of a wavelength. To meet the stability criteria, the temporal step is given by

$$\Delta t<\frac{\Delta x}{\max_{\vec{r}}\left[c_0\left(\vec{r}\right)\right]\sqrt{3}},$$

where Δx is the spatial step of the grid. For example, for a 5-kHz simulation, the temporal step was set to $\Delta t = 0.0054$ μs. Speed of sound and density maps were extracted from the high-resolution tomography images. The mean computation time was 18 h.

Numerical Simulation in Finite Elements Oral Cavity. The resonance frequencies of the oral and nasal cavities, as well as of the open nostrils, were computed by a finite-element approach. The resonance frequencies and the associated pressure distribution are the eigenvalue and eigenvector for the following eigenvalue problem: $[\mathbf{K} - \omega 2\mathbf{M}]\{p\} = 0$ associated with Neumann boundary condition ($dp/dn = 0$ on the surface of the volume mesh) wherein matrices [**K**] and [**M**] are the acoustic stiffness and mass matrix, respectively, and $\omega = 2\pi f$, with f as the frequency. Computations were performed using LMS Sysnoise (LMS).

Data Analysis. The density of soft tissue values in an earless frog (Sooglossidae, $n = 4$) and an eared frog (Eleutherodactylidae, $n = 3$) was compared. A two-way repeated-measures ANOVA was conducted on the tissue density data in SPSS (IBM SPSS V. 20).

ACKNOWLEDGMENTS. We thank the Seychelles Bureau of Standards for permission to work on the Silhouette Island, Republic of Seychelles, the R. Gerlach family (Nature Protection Trust of Seychelles), and L. Chong Seng for assisting during fieldwork. We also thank the team of the Centre de Microscopie de fluorescence et d'IMagerie numérique du Muséum (CeMIM) (M. Gèze and M. Dellinger, Muséum national d'Histoire naturelle) for allowing us to use the graphics workstation. We thank M. Tanter (Institut Langevin) for allowing us to use his 3D finite differences code. We are grateful to the Ministry of Environment of Seychelles and its Principal Secretary Mr. D. Dogley for providing collecting permits used for the specimens mentioned in this paper. Finally, we thank J. M. Boistel, M. Boistel, M. Goyon, A. Mazabraud, E. Boller, F. Guy, A. Herrel, P. Tafforeau, J.-Y. Tinevez, and the teams of ID19 at the ESRF for help. The European Synchrotron Radiation Facility is acknowledged for providing beamtime in the framework of Proposals SC-1593 and MD179.

1. Schnupp JWH, Carr CE (2009) On hearing with more than one ear: Lessons from evolution. *Nat Neurosci* 12(6):692–697.
2. Allen J (1985) Cochlear modeling. *IEEE ASSP Mag* 2(1):3–20.
3. Clack JA (1989) Discovery of the earliest-known tetrapod stapes. *Nature* 342(6248): 425–427.
4. Van Bergeijk WA (1966) Evolution of the sense of hearing in vertebrates. *Am Zool* 6(3):371–377.
5. Jaslow AP, Hetherington TE, Lombard RE (1988) *The Evolution of the Amphibian Auditory System*, eds Fritzsch B, Ryan MJ, Wilczynski W, Hetherington TE, Walkowiak W (Wiley, New York), pp 69–91.
6. Estrada AR, Hedges SB (1996) At the lower size limit in tetrapods: A new diminutive frog from Cuba (Leptodactylidae: *Eleutherodactylus*). *Copeia* 1996(4):853–859.
7. Van der Meijden A, et al. (2007) Molecular phylogenetic evidence for paraphyly of the genus *Sooglossus*, with the description of a new genus of Seychellean frogs. *Biol J Linn Soc Lond* 91(3):347–359.
8. Biju SD, Bossuyt F (2003) New frog family from India reveals an ancient biogeographical link with the Seychelles. *Nature* 425(6959):711–714.
9. Nussbaum RA, Jaslow AP, Watson J (1982) Vocalization in frogs of the family Sooglossidae. *J Herpetol* 16(3):198–203.
10. Gerlach J, Willi J (2002) A new species of frog, genus *Sooglossus* (Anura, Sooglossidae) from Silhouette Island, Seychelles. *Amphib-reptil* 23(4):445–458.
11. Mason MJ (2006) *Hearing and Sound Communication in Amphibians. Springer Handbook of Auditory Research,* eds Narins PM, Feng AS, Fay RR, Popper AN (Springer, New York), pp 147–183.
12. Hetherington TE, Lindquist ED (1999) Lung-based hearing in an "earless" anuran amphibian. *J Comp Physiol A Neuroethol Sens Neural Behav Physiol* 184(4):395–401.
13. Lombard RE, Straughan IR (1974) Functional aspects of anuran middle ear structures. *J Exp Biol* 61(1):71–93.
14. Hetherington TE (1992b) The effects of body size on the evolution of the amphibian middle ear. *The Evolutionary Biology of Hearing*, eds Webster DB, Fay RR, Popper AN (Springer, New York), pp 421–437.
15. Nuzzo S, Peyrin F, Cloetens P, Baruchel J, Boivin G (2002) Quantification of the degree of mineralization of bone in three dimensions using synchrotron radiation microtomography. *Med Phys* 29(11):2672–2681.
16. Martín-Badosa E, et al. (2003) A method for the automatic characterization of bone architecture in 3D mice microtomographic images. *Comput Med Imaging Graph* 27(6):447–458.
17. Berger EH, Kieper RW, Gauger D (2003) Hearing protection: Surpassing the limits to attenuation imposed by the bone-conduction pathways. *J Acoust Soc Am* 114(4 Pt 1): 1955–1967.
18. Nadrowski B, Martin P, Jülicher F (2004) Active hair-bundle motility harnesses noise to operate near an optimum of mechanosensitivity. *Proc Natl Acad Sci USA* 101(33): 12195–12200.
19. Martin P, Hudspeth AJ (2001) Compressive nonlinearity in the hair bundle's active response to mechanical stimulation. *Proc Natl Acad Sci USA* 98(25):14386–14391.
20. Aertsen AM, Vlaming MS, Eggermont JJ, Johannesma PI (1986) Directional hearing in the grassfrog (Rana temporaria L.). II. Acoustics and modelling of the auditory periphery. *Hear Res* 21(1):17–40.
21. Palmer AR, Pinder AC (1984) The directionality of the frog ear described by a mechanical model. *J Theor Biol* 110(2):205–215.
22. Lieberman P (1977) *Speech Physiology and Acoustic Phonetics* (Macmillan Pub Co, New York), pp 1–208.
23. Nowicki S (1987) Vocal tract resonances in oscine bird sound production: evidence from birdsongs in a helium atmosphere. *Nature* 325(6099):53–55.
24. Boistel R, et al. (2011) Whispering to the deaf: Communication by a frog without external vocal sac or tympanum in noisy environments. *PLoS ONE* 6(7):e22080.
25. Lewis ER (1984) On the frog amphibian papilla. *Scan Electron Microsc* 4:1899–1913.
26. Loftus-Hills JJ (1973) Neural mechanisms underlying acoustic behaviour of the frog *Pseudophryne semimarmorata* (Anura: Leptodactylidae). *Anim Behav* 21(4):781–787.
27. Jaslow AP, Lombard RE (1996) Hearing in the neotropical frog, *Atelopus chiriquiensis. Copeia* 1996(2):428–432.
28. Lindquist ED, Hetherington TE, Volman SF (1998) Biomechanical and neurophysiological studies on audition in eared and earless harlequin frogs (*Atelopus*). *J Comp Physiol A Neuroethol Sens Neural Behav Physiol* 183(2):265–271.
29. Narins PM, Ehret G, Tautz J (1988) Accessory pathway for sound transfer in a neotropical frog. *Proc Natl Acad Sci USA* 85(5):1508–1512.
30. Heterington TE (1989) Vertebrate Morphology: Trends in vertebrate morphology. eds Splechtna H, Hilgers H (Gustav Fischer Verlag: Stuttgart, West Germany), pp 356–359.
31. Gould SJ, Vrba ES (1982) Exaptation: A missing term in the science of form. *Paleobiology* 8(1):4–15.
32. Laurin M, Germain D, Steyer J-S, Girondot M (2006) Données microanatomiques sur la conquête de l'environnement terrestre par les vertébrés. *C R Palevol* 5(3-4):603–618.
33. Clack JA, et al. (2003) A uniquely specialized ear in a very early tetrapod. *Nature* 425(6953):65–69.
34. Brazeau MD, Ahlberg PE (2006) Tetrapod-like middle ear architecture in a Devonian fish. *Nature* 439(7074):318–321.
35. Laurin M (1998) The importance of global parsimony and historical bias in understanding tetrapod evolution. Part I. Systematics, middle ear evolution and jaw suspension. *Ann Sci Nat Zool* 19(1):1–42.
36. Clack JA (2002) Patterns and processes in the early evolution of the tetrapod ear. *J Neurobiol* 53(2):251–264.
37. Ruta M, Coates MI, Quicke DLJ (2003) Early tetrapod relationships revisited. *Biol Rev Camb Philos Soc* 78(2):251–345.
38. Aubin T (1994) Syntana: A software for the synthesis analysis of animal sounds. *Bioacoustics* 6(1):80–81.
39. Guigay JP, Langer M, Boistel R, Cloetens P (2007) Mixed transfer function and transport of intensity approach for phase retrieval in the Fresnel region. *Opt Lett* 32(12):1617–1619.
40. Labiche JC, et al. (2007) Invited article: The fast readout low noise camera as a versatile x-ray detector for time resolved dispersive extended x-ray absorption fine structure and diffraction studies of dynamic problems in materials science, chemistry, and catalysis. *Rev Sci Instrum* 78(9):091301–091311.